

Effects of γ -ray irradiation and thermal annealing on structural, optical and electrical properties of vacuum deposited vanadyl 2,3-naphthalocyanine thin films

Nisha S. Panicker · C. S. Menon

Received: 9 November 2010 / Accepted: 27 January 2011 / Published online: 12 February 2011
© Springer Science+Business Media, LLC 2011

Abstract Vacuum deposited vanadyl naphthalocyanine (VONc) crystalline thin films were produced. The films showed a completely different structural and growth pattern on thermal annealing and γ -ray irradiation. The XRD spectra revealed polycrystalline nature for both annealed and γ -ray irradiated films. Raman spectra observes that the γ -irradiated films had a higher disorder producing broad and diffuse peaks in comparison to its annealed samples. In the absorption spectra, the γ -irradiated films shows a broad Q-band with a shift of 50 nm towards the IR region enabling VONc to be used in a lot of applications using the commercially available semiconductor NIR lasers. Films on 97.9 krad γ -ray irradiation showed some interesting properties with a better conductivity compared to either it's higher γ -ray irradiated counterpart (195.8 krad) or the annealed films. Also the activation energy values, which is the minimum amount of energy required to liberate charge carriers from traps or to ionize levels within the band gap, was found to be lowered to half of its value for the films irradiated at 97.9 krad promising its performance in optical data recording, photo-sensitizer in photodynamic therapy, etc.

Introduction

Metal naphthalocyanines (MNC) are promising candidate materials for the application of gas sensors, optical logic displays, solar cells, colour filters, imaging, data storage,

etc. [1–6]. Phthalocyanines (Pc) and naphthalocyanines are structural analogues of porphyrin with the pyrrole inner ring system joined together by aza ($-N=$) groups. Most of the properties of Pc and naphthalocyanines depend on π -electron conjugation in the macrocyclic ring. Recently, MNC's found its potential in the field of optical data recording media [2], in such a storage device a laser source is used to record minute optically detectable effects in thin film substrates such as change in reflectance and/or in light transmission by fusing, sublimation, vaporization, etc. Not many dyes are known to have high-optical extinction in the spectral range of available high-power injection lasers (750–900 nm), however, vanadyl naphthalocyanine (VONc) is a strong candidate for such a device due to their extended π -electron conjugated systems with additional benzoannulation causing the absorption band to shift towards IR region (shift towards the operating wavelength of the commercially available semiconductor lasers). Apart from their strong absorption in the near-infrared region, minimum thermal conductivity and enthalpy of melting per volume, excellent heat, light and chemical stability makes them well suited for use as storage layers [7]. In addition to such optical properties the electrical conductivity of the MNC could be tuned by using suitable central metal atom substitutions [5, 6] for its application in various semiconductor devices.

In this article, we have carried out a comparative study of γ -ray irradiation and thermal annealing effects on the structural, optical and electrical properties of vacuum-deposited VONc thin films. The properties of the film could be altered with thermal annealing due to the compaction/rearrangement within the film structure [8], while irradiation with γ -rays can induce structural defects otherwise known as colour centres due to the electron-defect linkage [9, 10].

N. S. Panicker · C. S. Menon (✉)
School of Pure and Applied Physics, Mahatma Gandhi University, Kottayam, Kerala 686560, India
e-mail: prof.menoncs@gmail.com

Materials and methods

Spectroscopic grade vanadyl 2,3 naphthalocyanine powder purchased from Sigma-Aldrich®, USA was used as the precursor for the preparation of thin films. Thin films of VONc were deposited on to quartz glass substrates with a Hind Hivac 12A4 coating unit using vacuum evaporation technique. Evaporation of the material is performed at a base pressure of 10^{-5} Pa from a molybdenum boat, which is used as the resistive heating element. Thicknesses of the films are measured by Tolansky's multiple beam interference technique. The deposited films were annealed at four different stages, namely, 323, 373, 423 and 473 K under normal atmospheric conditions. The films were γ -irradiated with a ^{60}Co γ source at three different dosages, namely, 195.8, 97.9 and 48.95 krad for 60 min.

The characterization of the prepared thin films were carried out with X-ray diffraction (XRD, model: PANalytical X'Pert PRO), Raman spectroscopy (Renishaw inVia), scanning electron microscopy (SEM, model: JEOL 5400), atomic force microscopy (AFM, WITec alpha 300A) and UV-Vis-NIR absorption spectroscopy (model: JASCO V570). The electrical measurements were carried out using a programmable Keithley electrometer (model No.617) for all the samples. To avoid any possible contamination, conductivity measurements were performed in vacuum at 0.133 Pa and in a dark chamber to reduce the photoconductive contribution of the molecules. Vacuum-deposited silver, with an interelectrode distance of 1 cm, was used as the ohmic contact for the films. The samples were mounted on the sample holder of the conductivity cell and the contacts were made with copper strands of diameter 0.6 mm using silver paste. The samples are heated using a resistive heating filament attached to the sample holder of the conductivity cell and the temperature in the conductivity cell is measured using a calibrated chromel-alumel thermocouple. Current to substrate heater is controlled by a variable voltage transformer and the substrate temperature was varied from 300 to 500 K with 5 K increments.

Results and discussion

Structural characterization

The thickness of the as-deposited films was found to be 600 nm on measurement by Tolansky's multiple beam interference technique [11]. After thermal annealing the thickness reduced to 450 nm owing to the heat compaction, but there was no substantial change in thickness for the films after γ -ray irradiation. The XRD characterization (Fig. 1) was carried out for the as-deposited, annealed (373

and 473 K) and γ -irradiated (195.8 krad) thin films. An XRD pattern of the VONc precursor used is also given for comparison in Fig. 1. The peaks observed in the as-deposited, annealed and γ -irradiated thin films correspond to its polycrystalline nature. The as-deposited sample and the one annealed at 373 K displayed few weak and diffuse crystal plane peaks, but at 473 K sharp peaks were revealed at 2θ values of 5.5°, 20.2°, 22.9° and 43.2°. The peak corresponding to 5.5° having a d -value of 15.9 Å was found stronger and broader compared to the others. It is evident that on heat treatment more peaks were revealed or either became intense/sharp which could be due to the removal of organic content within the film enabling a more facile arrangement of crystal planes. From the earlier reports on crystallization of VONc, very close d -values at 15.7 and 15.8 Å with a nearly square pattern along with a d -value of 3.8 Å was found while determining its unit cell dimensions [12]. Being larger π systems 2,3-naphthalocyanines are expected to have higher aggregation tendency and could possibly aggregate in a stacked or co-facial or in both orientations resulting in smaller crystal spacing [13] as observed at 4.38 Å (20.2°), 3.8 Å (22.9°) and 2.09 Å (43.2°). The γ -ray irradiated (195.8 krad) thin film, however, evolved to have a different crystalline orientation with major peaks at 23.6 Å (3.75°) and 17.1 Å (5.15°), corresponding to an orthogonal lattice arrangement as understood from the previous reports [14].

Raman spectra (Fig. 2) were measured for the samples as-deposited, annealed (473 K) and γ -irradiated at 195.8 krad. All samples gave a peak at 1582 cm^{-1} corresponding to their naphthalene ring back bone [15]. A strong and sharp peak at 1610 cm^{-1} found in the as-deposited and annealed sample could be attributed to the vCN and vCC vibrations [16]. The as-deposited film in comparison to the

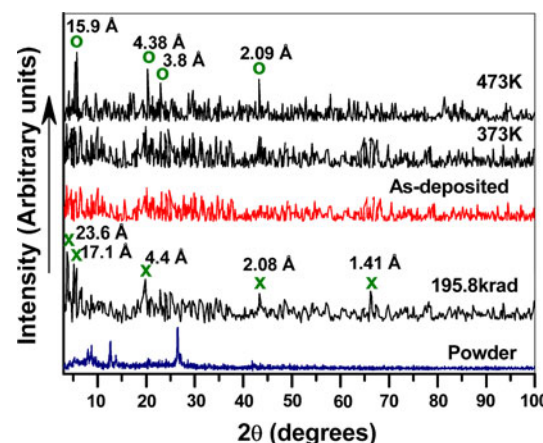


Fig. 1 (Colour online) XRD spectra for samples annealed at 373 and 473 K, and γ -irradiated at 195.8 krad along with the spectra of as-deposited and precursor powder

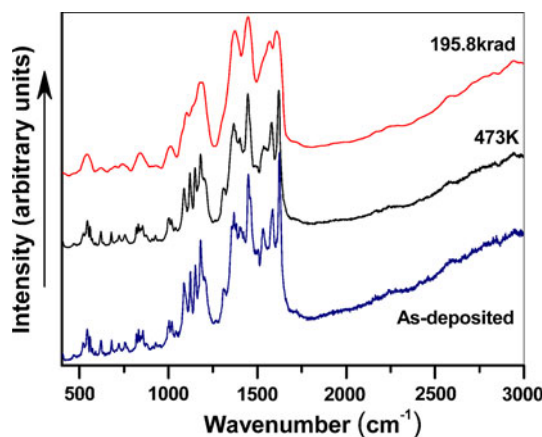


Fig. 2 (Colour online) Raman spectra for samples as-deposited, annealed at 473 K, and γ -irradiated at 195.8 krad

annealed and the γ -irradiated films showed more additional vibrations within the region 1250–1500 cm^{-1} due to the higher organic content within the film. The 1529 cm^{-1} vibration was found much stronger in the as-deposited film and is assigned to the ν -isoindole ring stretching [16]. The vibrations observed in the γ -irradiated sample are significantly reduced in comparison to the annealed sample and are also seen diffused around the 1594–1630 cm^{-1} region. Besides this observation, peaks which are sharp for annealed sample are found diffuse for the γ -irradiated films. The heat treatment could burn off most of the organic content within the film leaving behind a narrow range of organic vibrations. While the broad and diffuse peaks for γ -irradiated films indicate a higher disorder existing within the film structure [9].

SEM and AFM were engaged for the surface morphological studies revealing few evident differences between the annealed and γ -irradiated sample. The SEM image of the as-deposited sample (Fig. 3a) shows some lamellar structures embedded within the entire film while the sample annealed at 473 K (Fig. 3b) shows a continuous grainy pattern with some spherical and lamellar structure scattered through out the matrix [12]. The γ -irradiated thin film SEM image (Fig. 3c) depicts an entirely different growth pattern from that of the annealed sample with some spherical microparticles which are loosely adhered. The γ -irradiated film structures are filled with microcracks forming sub-microisland like structures. AFM image of the annealed sample (Fig. 4a) reveal that the lamellar structures, which were found in the SEM images, to be elongated microcrystals co-existing with the spherical ones, the inset of Fig. 4a shows its two-dimensional plateau. The γ -irradiated films (Fig. 4b) consist of spherical submicron particles with size ranging around 200–350 nm which is clearly seen in the Fig. 4b inset.

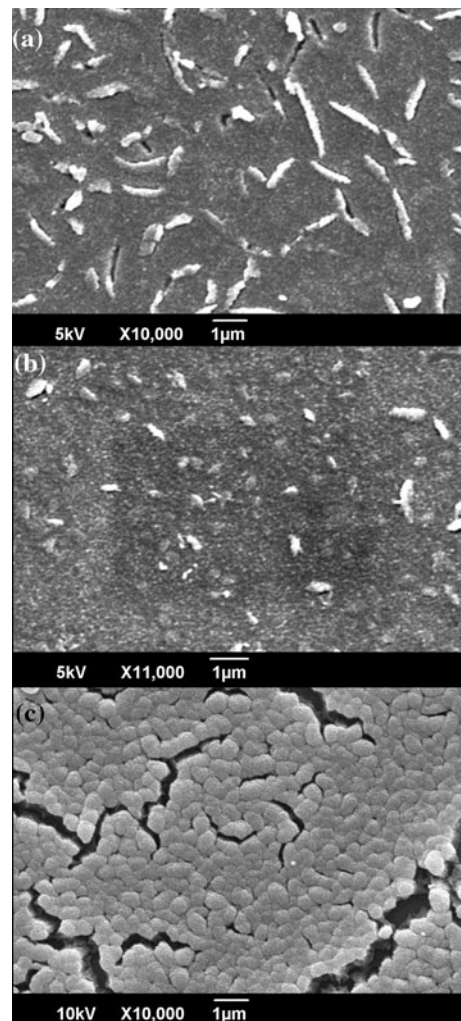


Fig. 3 Scanning electron micrograph of **a** as-deposited thin film, **b** film annealed at 473 K and **c** film γ irradiated at 195.8 krad

Optical characterization

The UV–Vis–NIR absorption spectroscopy points out another major difference between the annealed and γ -irradiated thin film in comparison to their as-deposited condition. Absorption spectra shown in Fig. 5 correspond to that of annealed films, while Fig. 6 corresponds to the γ -irradiated films. For as-deposited and annealed samples an intense Q-band arising from the direct electronic transitions between orbitals with a shoulder vibronic (Q_{vib}) band is clearly visible [17]. The Q-band for as-deposited thin film is found at 814 nm while on annealing at 473 K it produces a bathochromic shift of 6 nm. The Q-band is strongly localized on the Nc-ring backbone which is quite sensitive to the environment of the molecule, so the shift could be attributed to the rearrangement of the molecules upon the removal of carbon compounds and the hydroxyl groups. Since there are vibrational levels associated to

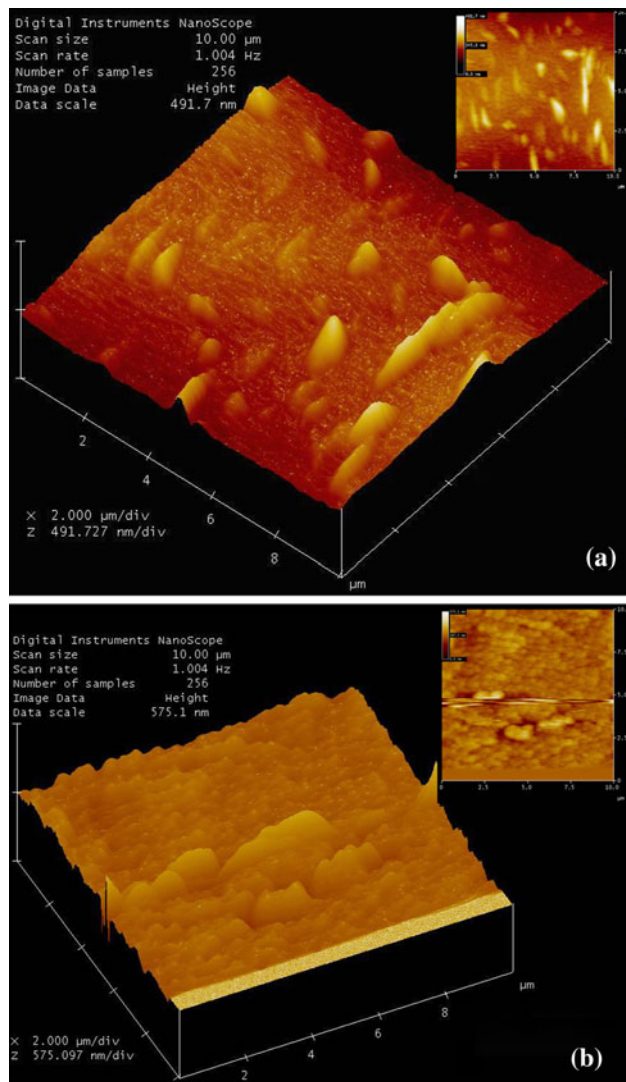


Fig. 4 Atomic force microscope images of **a** film annealed at 473 K and **b** film γ irradiated at 195.8 krad. The *inset* corresponds to its two-dimensional plateau

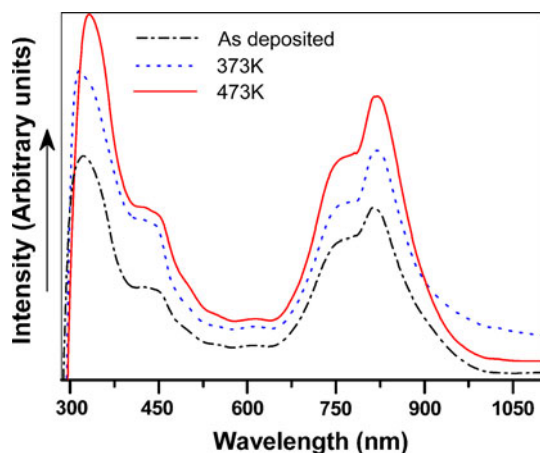


Fig. 5 UV-Vis-NIR spectra for the as-deposited sample and samples annealed at 373 and 473 K

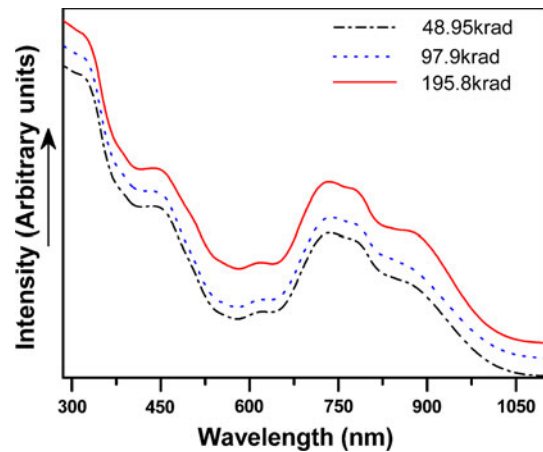


Fig. 6 UV-Vis-NIR spectra for the samples γ -irradiated at 48.95, 97.9 and 195.8 krad

every electronic level, the shoulder found at 761 nm is the Q_{vib} band indicated by its intensity which is 25% less than the main band [11, 18]. The γ -irradiated films gave a completely different Q-band signature in comparison to the as-deposited and the annealed films, the spectrum for 48.95 krad γ -ray irradiation is additionally provided for better comparison. The peaks were found at 732, 775, and 870 nm, an explanation could be given in association to the clustering behaviour found in the SEM. The γ -ray irradiation can bring about some symmetry breaking and induce the formation of dimeric species which is a probable result in clustered particles confronted by the strong aggregation tendency of 2,3-naphthalocyanines [9, 13]. This result is again substantiated by the previous reports predicting the formation of dimers reducing the strong Q-band peak of its monomer form [19]. Thus, the shift of the Q-band spectra from 820 nm on annealing, to 870 nm on γ -ray irradiation enables VONc to be used in a lot of applications due to the improved tuning towards the solar spectrum. Also as discussed in detail in the introduction, applications in data storage devices requires strong absorptance towards the emission wavelengths of existing and commercially available semiconductor lasers, namely, GaAlAs laser diodes (750–850 nm), Ti:sapphire laser (670–1,130 nm), Cr:Li-SAF solid-state dielectric laser (800–1,050 nm), InGaAs laser (900–1,065 nm), etc. [5, 20, 21].

Two charge transfer band was found between the Q-band and Soret band at 434 and 613 nm for all the samples irrespective of the processing conditions. Such types of bands were earlier reported for Pc when the metal d -orbitals lie within the HOMO–LUMO gap of the Pc ring [22]

The higher wavelength side of the Soret band was used to calculate the band gap energy. Figure 7a and b shows the $\alpha^2 - h\nu$ plot of all the samples and their x intercepts gives the value of the band gap [23]. As observed from the

intercept values, the band gap energy reduced on annealing from its as-deposited values of 3.15–2.92 eV (Fig. 7a) which might be due to the shift in the relative positions of the valence and conduction bands due to temperature dependence of dilatation of the lattice and/or electron-lattice interaction [24]. Also, on γ -ray irradiation the band gap energy reduced a bit to 3.07 eV (Fig. 7b) but remains stable for all irradiation dosage. Since the γ -ray irradiation bring about disorder within the film matrix by inducing structural defects which could broaden the localized and extended states creating a smaller energy band gap [1, 9].

The change in the band gap with temperature was quite linear and can be expressed as [24]:

$$E_g(T) = E_{g0} + \beta T \quad (1)$$

E_{g0} being the absolute zero value of the band gap and β is the rate of change of band gap with temperature. The values obtained were $E_{g0} = 3.55$ eV and $\beta = -1.35 \times 10^{-3}$. The negative β value signifies the shifting of band gap towards lower energies with an increase in annealing temperature, this indicates that the temperature affects the band gap by changing interatomic distances. The reduction rate in the band gap could be attributed to shortening of interatomic distances caused by the amplitude decrease of atomic oscillations around their equilibrium positions, and/or due to electron-lattice interaction which is dominant at elevated temperatures. The decrease in energy band gap increases the width of the energy bands which induce to move the band edge of the conduction band downward and that of the valence band upward. A successful model to predict the correct low-temperature dependence of the absorption edge and therefore derive the Urbach's rule [25] in the whole temperature range consider that the crystal should be divided into microscopic cells of the size of unit cell and the atoms in the different unit cells are independent of each other. Hence, each of the unit cell give similar contributions and the absorption coefficient for the whole crystal describes an exponentially increasing absorption edge below the band gap. This absorption tail arises from the thermal fluctuations in the band gap energy

of which the temperature dependence of the steepness parameter σ_0 is more accurately obtained in this specific model and is given by [26]

$$\frac{dE_g}{dT} = \frac{3k_B}{\sigma_0} \quad (2)$$

The σ_0 for the thin film was calculated from the slope of the band gap versus temperature curve via Eq. 2 and is found to be 0.1914.

Electrical conductivity studies

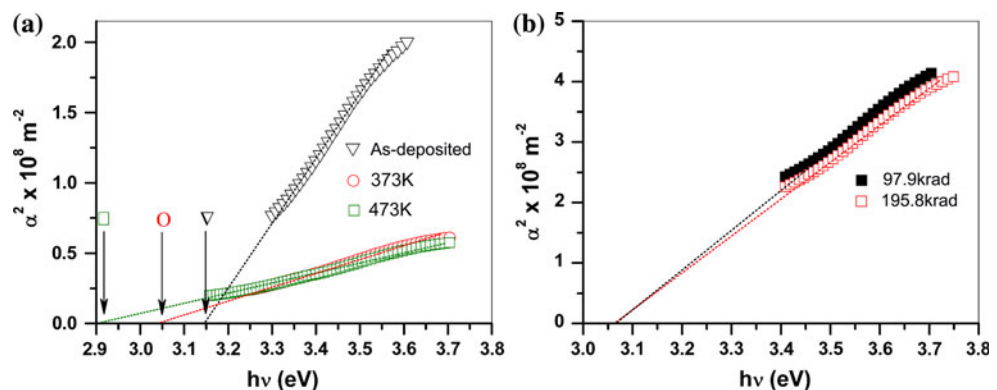
The thermal activation energy, E , which determines the minimum energy required to produce a charge carrier in the solid matrix, is calculated from the electrical conductivity data to understand the conduction mechanism in VONc thin films upon air annealing and γ -ray irradiation. Nc conductance arises from two factors (i) due to the π -orbital overlap of neighbouring molecules which are responsible for large number of acceptor/donor states injecting holes/electrons into the valence band and (ii) due to a higher anisotropy of lattice owing to low symmetry of metal-substituted Nc's. It was previously reported that the hopping process is mainly responsible for the conduction in such polycrystalline semiconductor organic molecules due to the weak van der Waals force interaction between them [27].

The electrical conductivity of the organic semiconductor obeys the Arrhenius equation thus the electrical conductivity σ can be expressed as:

$$\sigma = \sigma_0 \exp\left(\frac{-E}{k_B T}\right)$$

σ is the conductivity at temperature T , E is the thermal activation energy, k_B is the Boltzmann constant and σ_0 is the pre-exponential factor. Plotting $\ln \sigma$ versus $1,000/T$ yielded a straight line whose slope can be used to determine the thermal activation energy of the film. Figures 8 and 9 plots the $\ln \sigma$ versus $1,000/T$ graphs for the all the heat treated and γ -irradiated samples, respectively.

Fig. 7 (Colour online) α^2-hv plot for samples **a** as-deposited and annealed at 373 and 473 K, **b** γ -irradiated at 97.9 and 195.8 krad



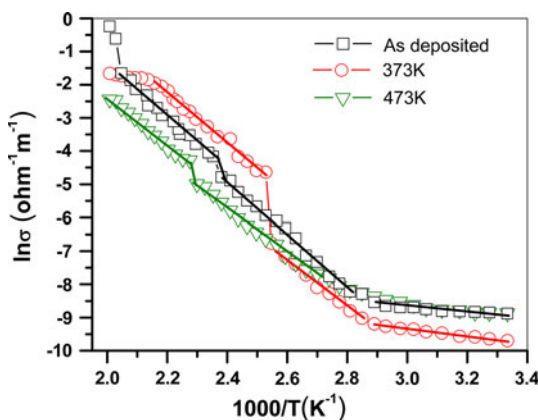


Fig. 8 (Colour online) $\ln\sigma$ vs. $1,000/T$ graph for as-deposited sample and samples annealed at 373 and 473 K

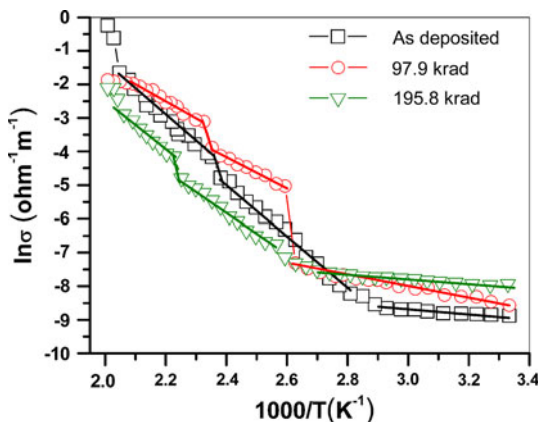


Fig. 9 (Colour online) $\ln\sigma$ vs. $1,000/T$ graph for samples γ -irradiated at 97.9 and 195.8 krad

Each curve contains three linear regions relating to the three activation energies E_1 , E_2 and E_3 and could be interpreted as the difference between dominant energy levels [28]. The change in the transport mechanism takes place due to a change in mobility of the charge carriers [29], in Pcs and NPs the conductivity is strongly temperature dependent and the charge carrier transport mechanism is generally of free band type in the higher temperature region and of hopping type in the low-temperature region [30]. There are several processes that can cause the conductivity in organic solids via Arrhenius type temperature dependence, few of which are (i) electron and hole production via thermal transition from a valence band to the conduction band where the increase of conductivity is dependant on the number of π -electrons. (ii) In materials with relatively large separation of excited levels, the conductivity may be due to thermal excitation of defect states that lies near the band edge, this extrinsic conductivity manifests itself in the breaks in the plot of $\ln\sigma$ versus

$1,000/T$. (iii) The band structure model can have some fluctuations of the potential well distribution in the crystal lattice due to perturbation caused by the disorders in the lattice causing a variation in the density of states from a critical to low value which are treated as localized states [31], but Mott [32] suggested an extended density of states with a long-range order in phase leading to the formation of tails in forbidden gap. (iv) When the concentration of disorder is high, Cohen et al. [33] suggested that the tails due to localized states originating from the conduction and valence bands can sometimes merge and overlap together forming localized states depending on the band gap, while Mott et al. [34] suggested a defect band due to the dangling/unsatisfied bonds leading to some local states called as pseudo-Fermi level regions.

Conductivity graphs are separately provided for annealed and γ -irradiated samples in comparison with the as-deposited stage. Conductivity for all the films was found to have much higher values, especially at the high-temperature region, from its previous report with a different sample preparation condition [35]. This indicates a production of large number of thermally activated charge carriers in vacuum-deposited films under investigation. From Fig. 8, it could be understood that the conductivity values for sample annealed at 373 and 473 K occupies a high and low values, respectively, in the high-temperature region whereas it almost get reversed at low-temperature region. Figure 9 represents the conductivity graph for γ -irradiated samples which shows that the samples irradiated at 97.9 krad has a higher conductivity values at the high-temperature region compared to the one irradiated at 195.8 krad. However, at the low-temperature region both samples shows much higher conductivity in comparison to the un-irradiated ones. The responsible factor for this change is solely due to the change in concentration of charge carriers induced by the irradiation energy [36]. Since the increase in irradiation dose can increase the generated number of electrons, a slightly higher conductivity values are observed for sample irradiated with 195.8 krad. Irradiation with γ -rays can change both the value of the electrical conductivity and its temperature dependence due to the creation of point defects by the direct interaction of Compton electrons with lattice atoms and by multiple collisions. Also, there are chances of formation of short lived free radicals upon irradiation. The higher conductivity values for a moderate γ -ray irradiation at 97.9 krad might be due to the weakening of interaction forces between atoms due to the introduction of lattice defects or due to the ionization effects leading to the presence of internal bias. However, at 195.8 krad γ -ray irradiation the induced defects might have recombined showing lower conductivity values [1, 37, 38].

The calculated activation energies from the slopes of the conductivity graphs are shown in Table 1. The activation energy corresponding to the higher temperature region (E_1) is associated with the resonant energy involved in a short lived excited state (intrinsic generation process) and the lower ones (E_2 and E_3) are associated with a short lived charge transfer between impurity and the complex (impurity conduction). A clear indication of lowering of activation energy is observed for the irradiated samples compared to the un-irradiated ones. E_1 and E_2 values are much lower for irradiated samples substantiating the argument of formation of lattice defects and/or creation of internal bias due to ionization effects [37, 38].

Conclusion

VONc thin films were prepared by vacuum deposition method. The prepared films were annealed at moderately high temperatures and also γ -irradiated with a dosage of 97.9 and 195.8 krad to study the variation of its structural, optical and electrical properties. The XRD of the films annealed at 473 K and γ -irradiated at 195.8 krad clearly showed a polycrystalline nature. Structural characterization of γ -irradiated films revealed a uniform morphology throughout the film while the annealed films were embedded with microcystallites of varying sizes well evident from the SEM and AFM images. The films under γ -ray irradiation produced a shift in absorption bands towards the IR region with a broad band between 650 and 900 nm compared to the annealed films, which is an important technological advantage such as wide tunability, better operating wavelength match with the commercially available IR lasers. All the films showed much higher conductivity at the high-temperature region compared to its previous report. It was found that under 97.9 krad γ -ray irradiation the film showed some interesting properties with a better conductivity compared to either its higher γ -irradiated counterpart (195.8 krad) or the annealed films. Finally, the values of activation energy, which is the minimum amount of energy

Table 1 Activation energies E_1 , E_2 , E_3 obtained for samples annealed/ γ -irradiated at various stages

Annealed/ γ -irradiated sample	Activation energy (eV)		
	E_1	E_2	E_3
300 K	0.6844	0.6637	0.0058
373 K	0.6287	0.5923	0.0531
473 K	0.6041	0.54592	0.0560
97.9 krad	0.3438	0.3302	0.0697
195.8 krad	0.6011	0.5325	0.0233

required to liberate charge carriers from traps or to ionize levels within the band gap, was found to be lowered to half of its value for the films irradiated at 97.9 krad thereby promising its performance in optical data recording, photosensitiser in photodynamic therapy, etc.

References

- Arshak A, Zleetni S, Arshak K (2002) Sensors 2:174
- Tomiyama T, Watanabe I, Kuwano A, Habiro M, Takane N, Yamada M (1995) Appl Opt 34:8201
- Kivits P, de Bont R, van der Veen J (1981) Appl Phys A 26:101
- Silva EAB, Borin JF, Nicolucci P, Graeff CFO, Ghilardi NT, Bianchi RF (2005) Appl Phys Lett 86:131902
- Wöhrle D, Meissner D (1991) Adv Mater 3:129
- Liljeroth P, Repp J, Meyer G (2007) Science 317:1203
- Ueno M, Yuasa T (1990) Infrared absorbing dyes. Plenum Press, New York
- Gaffo L, Cordeiro MR, Freitas AR, Moreira WC, Girotto EM, Zucolotto V (2010) J Mater Sci 45:1366. doi:[10.1007/s10853-009-4094-3](https://doi.org/10.1007/s10853-009-4094-3)
- Yaghmour SJ (2009) J Alloys Compd 486:284
- El-Batal FH (2008) J Mater Sci 43:1070. doi:[10.1007/s10853-007-2254-x](https://doi.org/10.1007/s10853-007-2254-x)
- Maissel LI, Glang R (1985) Handbook of thin film technology. McGraw Hill, New York
- Yanagi H, Ashida M, Elbe J, Wohrle D (1990) J Phys Chem 94:7056
- Tai S, Hayashi N (1991) J Chem Soc Perkins Trans 2:1275
- Manivannan A, Nagahara LA, Hashimoto K, Fujishima A, Yanagi H, Kouzeki T, Ashida M (1993) Langmuir 9:771
- Jiang J, Arnold DP, Yu H (2000) Polyhedron 19:1381
- Carrasco EAF, Campos-Valette M, Saavedra MS, Diaz GF, Clavijo RE, Garcia-Ramos JV, Sanchez-Cortes S (2001) Vib Spectrosc 26:201
- Kadish KM, Smith KM, Guillard R (2003) The porphyrin handbook: vol 16 phthalocyanines: spectroscopic and electrochemical characterization. Academic Press, California
- El-Nahassa MM, Abd-El-Rahman KF, Al-Ghamdib AA, Asiri AM (2004) Physica B 344:398
- Tai S, Hayashi N (1991) J Chem Soc Perkin Trans 2:1275
- Day P (2010) Physica B 405:S6
- Minh LQ, Chot T, Dinh NN, Xuan NN, Bingh NT, Phuoc DM (1987) Phys Stat Solidi A 101:K143
- Chen Y, Hanack M, Blau WI, Dini D, Liu Y, Lin Y, Bai J (2006) J Mater Sci 41:2169. doi:[10.1007/s10853-006-5552-9](https://doi.org/10.1007/s10853-006-5552-9)
- Collins RA, Krier A, Abass AK (1993) Thin Solid Films 229:113
- Yakuphanoglu F, Arslan M, Küçükislamoğlu M, Zengin M (2005) Sol Energy 79:96
- Urbach F (1953) Phys Rev 92:1324
- Skettrup T (1978) Phys Rev B 18:2622
- Schön JH, Kloc Ch, Batlogg B (2001) Phys Rev Lett 86:3843
- Belghachi A, Collins RA (1988) J Phys D 21:1647
- Gould RD (1996) Coord Chem Rev 156:237
- Vidadi YA, Rozenstein LD, Chistyakov EA (1969) Sov Phys Sol Stat 11:219
- Anderson PW (1985) Phys Rev 109:1492
- Mott NF (1967) Adv Phys 16:49
- Cohen NH, Fritche H, Ovshinsky SR (1969) Phys Rev Lett 22:1065
- Mott NF, Davis EA (1970) Phil Mag 22:903

35. Thomas J, Pillai VNS, Nampoori VPN, Vallabhan CPG (1999) *J Mater Sci Lett* 18:963
36. El-Nahass MM, Farag AAM, Atta AA (2009) *Synth Met* 159:589
37. Ahmed MA, Summan AM, Mousa MA (1992) *J Mater Sci-Mater Electron* 2:1
38. Gaffar MA, Hussien AG (2001) *J Phys Chem Solids* 62:2011